Powder Injection Molding of Ceria-Stabilized, Zirconia-Toughened Mullite Parts for UAV Engine Components

RENEE MARTIN,[1] MICHAEL VICK,[2] RAVI K. ENNETI,[3,4] and SUNDAR V. ATRE[1]

1.—Oregon State University, 204 Rogers Hall, Corvallis, OR 97331, USA. 2.—Naval Research Laboratory, 4555 Overlook Ave SW, Washington, DC 20375, USA. 3.—Global Tungsten and Powders Corp, 1 Hawes Street, Towanda, PA 18848, USA. 4.—e-mail: ravi.enneti@globaltungsten.com

Powder injection molding (PIM) of ceria-stabilized, zirconia-toughened mullite composites were investigated in the present article with the goal of obtaining performance enhancement in complex geometries for energy and transportation applications. A powder-polymer mixture (feedstock) was developed and characterized to determine its suitability for fabricating complex components using the PIM process. Test specimens were injection molded and subsequently debound and sintered. The sintered properties indicated suitable properties for engine component applications used in unmanned aerial vehicles (UAVs). The measured feedstock properties were used in computer simulations to assess the mold-filling behavior for a miniature turbine stator. The results from the measurements of rheological and thermal properties of the feedstock combined with the sintered properties of the ceria-stabilized, zirconia-toughened mullite strongly indicate the potential for enhancing the performance of complex geometries used in demanding operating conditions in UAV engines.

INTRODUCTION

Significant research efforts are being focused currently on developing material systems and manufacturing processes to produce enhanced performance parts made from ceramics. The properties of ceramics such as light weight, high temperature stability, high creep resistance, low thermal coefficient of expansion, chemical stability, and high strength at elevated temperatures make them strong candidates for applications such as miniature engine components for unmanned aviation vehicles and portable power generation. The use of ceramic parts made for these applications will enable a higher operating temperature resulting in enhanced performance and efficiency. For example, an increase in efficiency of greater than 10% has been previously reported by coating various engine components with ceramics.[1–3] However, the requirement of complex-shaped, precision parts for these applications is a major barrier in taking advantage of enhanced properties provided by ceramics. The high hardness of the ceramics makes machining the complex parts difficult and expensive, thus, minimizing the available manufacturing options to produce the parts economically.[4–8] Powder injection molding (PIM), as a result of its ability and proven record of manufacturing net shape complex parts economically, is identified as a suitable choice to produce complex ceramic parts.

Over the past few decades, PIM has experienced significant growth as a result of its inherent ability to manufacture large volumes of near net shape complex parts economically.[9–12] These unique characteristics of PIM resulted in the practice of the technology in manufacturing parts with complex shape and enhanced property requirements in widespread applications such as automotive, defense, electronic, medical, etc. In PIM, the shaping of the parts is carried out with an injection molding machine using a mixture of ceramic/metal powders and polymers (binder). After shaping, the polymer is removed and the part is heated to a high temperature under a controlled atmosphere to obtain the desired microstructure and properties.

The success of using PIM to manufacture complex parts with enhanced properties strongly depends on

the ability to develop optimized powder-binder (feedstock) compositions. The use of optimized feedstocks as starting materials will enable successful processing and producing defect-free parts with enhanced properties that are required for the intended critical applications.[4–7] The emphasis on feedstock properties becomes more important as a result of the complex shape of the parts that require good flow of the materials during the mold-filling phase of PIM.

Our prior publication discussed the ability of PIM to manufacture complex shape engine components for transportation from silicon nitride.[1] The measured feedstock properties were used to simulate the flow of the material during injection molding. The areas susceptible for formation of defects were also identified during the simulations. Owing to their relatively lower cost and sintering temperature, it is anticipated that ceria-stabilized, zirconia-toughened mullite composites could have a decided advantage over silicon nitride in fabricating complex-shaped enhanced property parts for ceramic engine applications in unmanned aviation vehicles.[13–16] Compared with mullite, zirconia-toughened mullite composites also show increased fracture toughness and creep resistance.

In this article, the use of PIM to manufacture complex-shaped parts with enhanced properties from zirconia-toughened mullite composite is presented. A new zirconia-toughened mullite feedstock was developed, and its properties were used to simulate the injection molding behavior of miniature turbine engine stators. The simulation results will assist in eliminating expensive and time-consuming trial-and-error practices currently prevalent in the PIM by selecting, developing, and optimizing various material and process parameters. The study confirmed the potential ability of PIM to manufacture complex-shaped parts requiring enhanced properties.

EXPERIMENTAL

Commercially available high-purity mullite (average particle diameter: 0.7 μm, and BET surface area 8.5 m^2/g) and ceria-stabilized zirconia (average particle diameter: 0.75 μm, and BET surface area 12.5 m^2/g) were used in the present study. Ceria was added to stabilize the high-temperature tetragonal or cubic phases of zirconia at room temperature. The scanning electron microscope (SEM) images of the as-received powders are shown in Fig. 1. A mixture of paraffin wax, polypropylene, linear low-density polyethylene, and stearic acid were used for the binder. The multicomponent system has a density of 0.873 g/cm^3. The two powders were mixed using an 80/20 vol.% mullite-to-ceria stabilized zirconia ratio via wet ball milling for 24 h in DI water, ammonia, and a dispersant (Darvan 821A, R.T. Vanderbilt Company, Inc.). Ceria-stabilized zirconia media were used. After milling, the
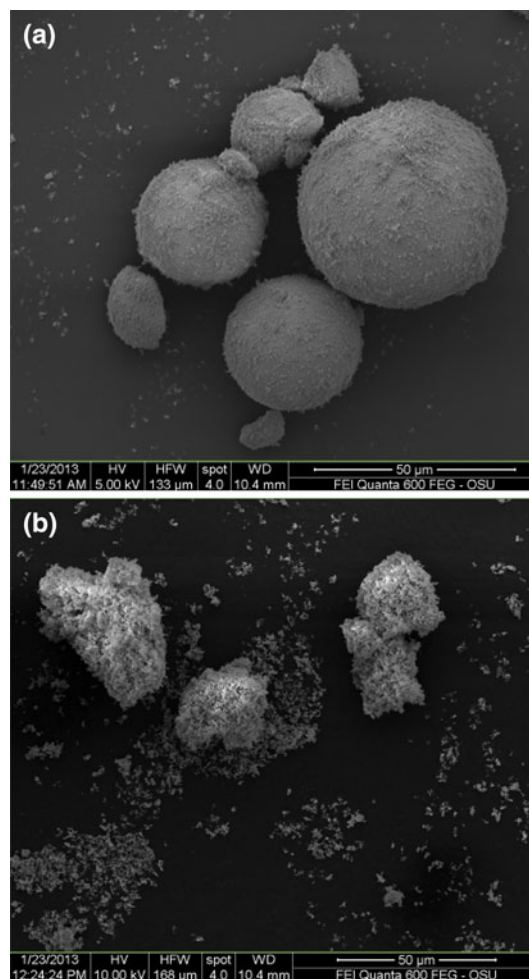

Fig. 1. Scanning electron micrographs of as-received (agglomerated) powders: (top) mullite and ceria-stabilized zirconia (bottom).

mixture was dried and heated to 550°C for dispersant removal. The resulting powder cake was ground and passed through a 45-mesh sieve. Feedstock compounding was carried out using an Entek co-rotating twin-screw extruder with an L/D ratio of 40 at ~85 wt.% solids loading. Rectangular coupons, of average dimensions 38 mm × 25 mm × 2 mm, were injection molded with six ~1-mm-wide slots. Molding was carried out on an Arburg 221 M molding machine. Samples were thermally debound and sintered at 1500°C for 4 h in a production furnace at Kyocera.

Simultaneous TGA/DSC was performed on feedstock pellets using a TA Instruments SDT Q600. Samples were run in nitrogen and clean, dry air (100 mL/min) from 30°C to 600°C at 10°C/min. Feedstock viscosity was measured by capillary rheometry (Rheograph 2003, Goettfert) in accordance with ASTM D3835. Tests were run between 150°C and 180°C at shear rates of 1 s^{-1}–10^6 s^{-1}. Thermal conductivity was measured using the transient line-source technique in accordance with ASTM D5930. Measurements were performed on a K-system II

thermal conductivity from 190°C to 30°C. A DSC (DSC7, Perkin Elmer) was used to determine the specific heat of the feedstock. Tests were performed in a nitrogen atmosphere (25 mL/min) from 190°C to 20°C with a cooling rate of 20°C/min. Volume change with temperature and pressure was studied through high-pressure dilatometry with a Gnomix PVT apparatus. The tests utilized the injection-molded parts, and the samples were heated at 3°C/min to 200°C. Sintered samples were polished to 0.1 μm and thermally etched at 1450°C for 5 h. The microstructure of the sintered parts was investigated using SEM. Vickers hardness was measured in accordance with ATSM C1327, and fracture toughness was measured via Vickers indentation.[17,18] The simulations of the injection molding process were carried out using Moldflow software (Autodesk Inc.).

RESULTS AND DISCUSSION

The TGA result of the feedstock in air and nitrogen atmospheres is shown in Fig. 2. The onset for burnout of the binders starts at approximately 180°C in both nitrogen and air. A higher rate of binder burnout is observed in air compared with nitrogen at temperatures above 250°C. Most of the binder (about 90 wt.%) is removed by 400°C in air. Inspection of the corresponding derivative curves showed an exothermic peak in air at 290°C that is absent in nitrogen. The release of heat during this combustion reaction speeds the degradation of the binder components in air.

Two distinct regimes, exhibiting the burnout of the low- (180°C–400°C) and high-molecular-weight components (400°C–550°C) of the binder system are observed in the TGA curves under nitrogen atmosphere. These regions are not as distinct in air. The heat released from combustion, as discussed earlier, allows the high-molecular-weight components to begin to burn off at lower temperatures and blurs the separation between the two types of binder
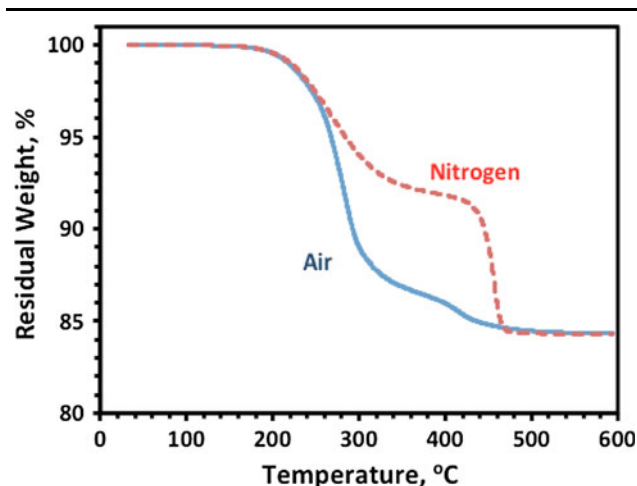
constituents. The observed breakdown behavior of the feedstock is used to construct the debinding schedule for thermal debinding of molded components. Both atmospheres can be used to completely thermally debind the material, although organic removal is completed at lower temperatures in nitrogen (~500°C) than in air (~550°C). A slower heating schedule in air is required to prevent defects resulting from rapid burnout between 250°C and 300°C.

The rheological behavior of the feedstock is shown in Fig. 3. The viscosity of the feedstock decreases with an increasing shear rate, demonstrating the pseudoplastic flow of the feedstock. This shear thinning behavior is a required property for successful injection molding. A feedstock that exhibits dilatant, or shear thickening, behavior will experience powder agglomeration and subsequent powder-binder separation during the molding process.[19,20] Furthermore, shear-thinning behavior has been shown to ease molding and reduce the occurrence of jetting.[20] Viscosities also fall within the moldable
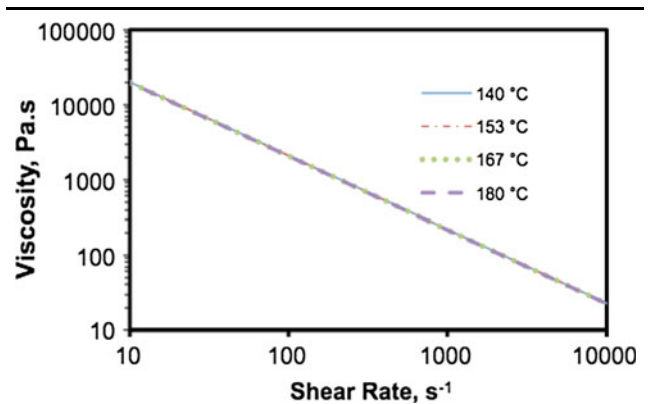
Fig. 3. Variation of viscosity of feedstock with shear rates at different temperatures.

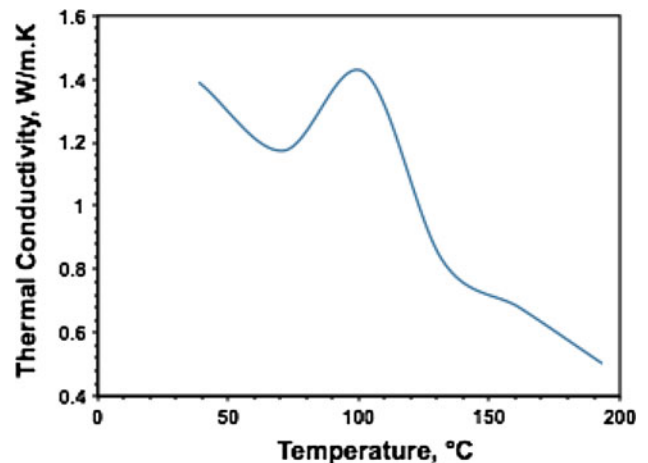Fig. 2. TGA results of the feedstock in air and nitrogen.

Fig. 4. Variation of thermal conductivity of feedstock with temperature.

range (less than 10^3 Pa s) for the shear rates typically experienced during molding (10^2 s^{-1}–10^5 s^{-1}), indicating processibility over the entire melt temperature range.[20,21] Furthermore, the feedstock viscosity is comparable with that of other ceramic feedstocks based on a wax-polymer binder system. For example, for a shear rate of 1000 s^{-1} at 160°C, the viscosity of the zirconia-toughened mullite

Fig. 5. Variation of specific heat of feedstock with temperature.

Fig. 6. Variation of specific volume of feedstock with temperature.

feedstock is ∼230 Pa s. This value falls within the range reported for silicon carbide and aluminum nitride feedstocks (∼100 Pa s–500 Pa s).[22] The differences in viscosity values can be attributed to the variations in particle characteristics.

The variation of thermal conductivity of the feedstock with temperature is shown in Fig. 4. The largest increase occurs between 132°C and 102°C, which corresponds to the onset of crystallization.[23] Other ceramic feedstocks showed similar behavior. A strong increase in the thermal conductivity has been observed between 125°C and 64°C for an alumina feedstock and between 184°C and 154°C for a silicon nitride feedstock.[1,24]

The variation in specific heat of the feedstock with temperature is shown in Fig. 5. Peaks in the data mark crystallization temperatures, and lower values indicate regions of faster cooling.[17] Specific heat is used along with thermal conductivity to determine the cooling behavior of the feedstock melt (i.e., flow front temperature, cooling time, etc.).[18] The results for the zirconia-toughened mullite feedstock are in qualitative agreement with other ceramic feedstocks. The peak in specific heat observed in the zirconia-toughened mullite feedstock at 50°C is analogous to the peaks observed at 46°C and 49°C for silicon carbide and aluminum nitride feedstocks, respectively.[22]

Figure 6 shows the pressure–volume–temperature (PVT) data for the zirconia-toughened mullite feedstock material. The sharp change observed in each curve marks the melting temperature at the given pressure and clearly separates the melt and solid domains. Melting temperatures are influenced by pressure and increase from approximately 64°C to 103°C as pressure increases from 0 MPa to 200 MPa. Volume does increases with temperature, but temperature has less of an effect on volume change as the pressure is increased. Information on the PVT behavior is used during the packing phase of the injection molding process to determine the amount of additional material to be added to ensure complete mold filling as the melt begins to cool and shrink.
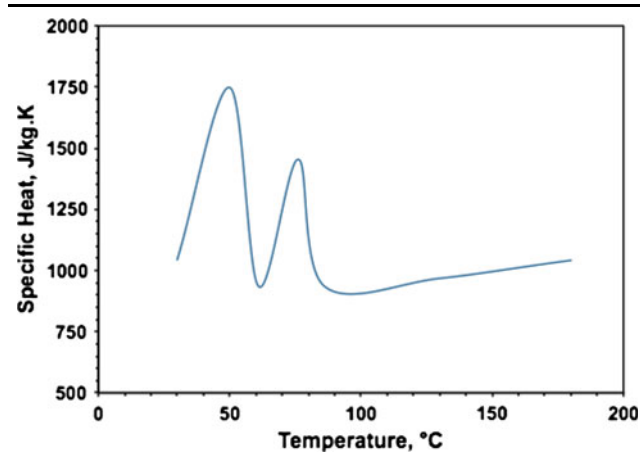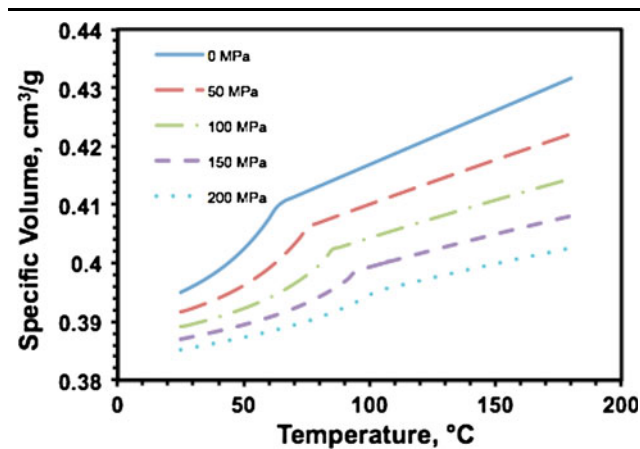
Table I. Representative properties of various ceramic feedstocks based on a wax-polymer binder system

| Reference	Material system	Filler content (wt.%)	Initial solid density (kg/m³)	Melt density (kg/m³)	Melt specific heat (J/kg·K)	Melt thermal conductivity (W/m K)	Transition temperature (°C)
This work	Zirconia-mullite	84	2520	2290	1040	0.7	81
24	Alumina	84	2580	2340	1300	1.4	52
21	Aluminum nitride	80.5	–	1940	1200	2.2	53
21	Aluminum nitride	85	–	2140	1410	2.9	53
1	Silicon nitride	80	2300	2110	1160	1.3	53
21	Silicon carbide	89.5	–	1950	1200	2.5	52
21	Silicon carbide	82	–	1990	1250	2.3	52
21	Wax-polymer binder	0	870	710	2590	0.2	99
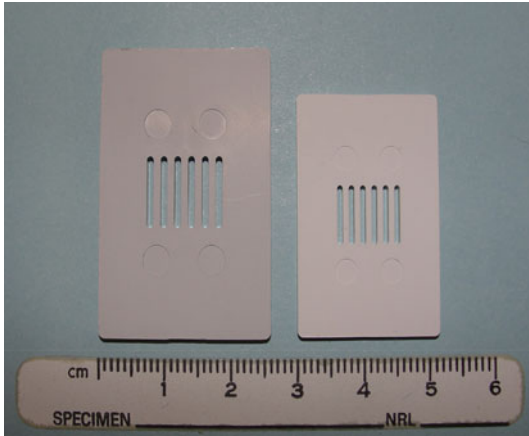
Fig. 7. Molded (left) and sintered (right) multislotted test coupon. The sample was sintered at 1500°C for 4 h to obtain a sintered density of 97.3% theoretical. A linear shrinkage of 16.5% was observed from the green to sintered stage.

Table I shows some representative properties of various ceramic feedstocks based on a wax-polymer binder system.

The binder system properties are also given for comparison. The sensitivity of feedstock behavior to the material system (i.e., filler material) can be determined from an examination of these properties. Melt and solid densities for all the feedstocks vary within a similar range of values (1940 kg/m^3– 2580 kg/m^3). Melt-specific heats also showed little variation (1040 J/kg K–1410 J/kg K) from filler to filler. Melt thermal conductivity, however, is clearly dominated by the thermal conductivity of the filler and varies widely from system to system (0.7 W/m K–2.9 W/m K). The transition temperature varies between 52°C and 53°C for all systems except for the zirconia-toughened mullite feedstock for which the transition temperature, 81°C, approaches that of the binder system, ~100°C. This behavior is perhaps explained by the relative similarity between the thermal conductivity behavior of the zirconia-toughened mullite feedstock and the binder system as compared with the other feedstock systems.

Trials were performed to confirm the moldability of the feedstock to shape parts with complex geometries. Test coupons with a series of six ~1-mm-wide slots were molded (Fig. 7) to evaluate the capability of the feedstock. A complete mold filling was achieved, and the obtained green parts showed no warpage, cracks, or surface defects.

After molding, the green parts were thermally debound and sintered in air. Sintered samples

Table II. Summary of the sintered properties of zirconia-toughened mullite

Property	
Density, (g/cm^3)	3.76
Final density, % theoretical	97.3
Linear shrinkage, (%)	16.5
Vickers hardness, (GPa)	11.8 ± 0.4
K_c, (MPa m$^{1/2}$)	4.3 ± 0.3

Table III. Summary of the composition, process conditions, and fracture toughness values of mullite-zirconia composites reported from prior studies

Composition	Process	Sintering conditions	Fracture toughness[a] (MPa m$^{1/2}$)	Reference
Mullite–20 vol.% Zr(Ce)O$_2$	PIM	1500°C, 4 h	4.3 ± 0.3	Present study
Al$_2$O$_3$—48.3 wt.%–64.9 wt.% ZrO$_2$	Slip casting, reaction sintered	1450–1600°C, 2 h	2.1–3.9	25
Mullite—0 vol.%–20 vol.% ZrO$_2$	Attrition milling isostatic pressing	1570°C, 2.5 h	2.1–3.2	26
Mullite—0 vol.%–32 vol.% ZrO$_2$	Uniaxial pressing	1600°C, 2 h	1.8–2.9	27
Mullite—5 vol.%–20 vol.% ZrO$_2$	Uniaxial pressing	1100–1600°C, 8 h	1.7–3.8	28
Alumina gel—45 wt.%–75 wt.%, Zircon—15 wt.%–45 wt.%, CeO$_2$—1.5 wt.%–4.5 wt.%, Al-10 wt.%	Wet interaction, Uniaxial pressing	1400–1600°C, 2 h	2–4	29
Mullite—53.5 wt.%–60 wt.%, 36 wt.%–40 wt.% ZrO$_2$, 0 wt.%–10 wt.% Y$_2$O$_3$	Attrition milling, uniaxial pressing	1500–1600°C, 2 h	3.7–3.9	30
Mullite—12.5vol.%–30 vol.% ZrO$_2$	Uniaxial pressing	1595°C, 3 h	2.4–3.1	31
Mullite—10 wt.% ZrO$_2$, 1 wt.% MgO	Uniaxial pressing, microwave sintered	1500°C	3.7 ± 0.4	32

[a]The range of fracture toughness values represents the lower and upper bounds of the mean values measured over a range of compositions and sintering conditions. The error bars reported in the literature are typically ±0.3 MPa m$^{1/2}$.

exhibited uniform shrinkage of $\sim$16.5% (see Fig. 7), signifying uniform packing density and feedstock homogeneity. The properties of the sintered parts are summarized in Table II.

It can be seen from Table II that a $\sim$97% dense, zirconia-toughened material with a fracture toughness (K_c) of 4.3 ± 0.3 MPa m$^{1/2}$ and a Vickers
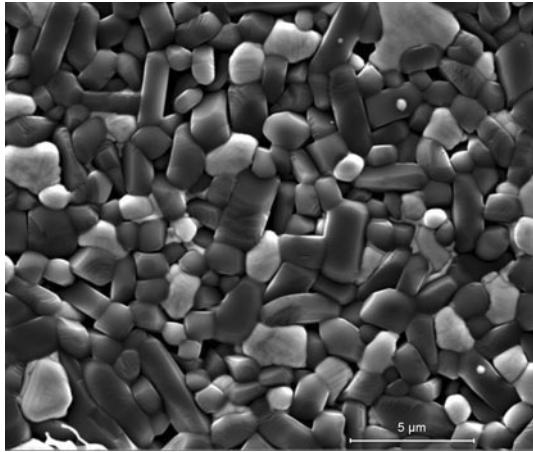

Fig. 8. Scanning electron micrograph for test coupon sintered at 1500°C for 4 h. The relatively dark regions represent mullite-rich grains, while the brighter regions represent zirconia-rich grains. The black regions are residual pores.

hardness of 11.8 ± 0.4 GPa was successfully obtained. In contrast, prior studies on mullite and zirconia-toughened mullite typically reported fracture toughness values of 2 MPa m$^{1/2}$–4 MPa m$^{1/2}$. The compositions, process conditions, and fracture toughness values of mullite-zirconia composites reported from prior studies are summarized in Table III.

The fracture toughness of the studies listed in Table III was measured using the Vickers indentation method. The fracture toughness values of mullite-zirconia composites for most of the prior studies was less than 4 MPa even after sintering at temperatures above 1500°C. In the present study, a fracture toughness (K_c) of 4.3 ± 0.3 MPa m$^{1/2}$ was achieved at sintering temperatures of 1500°C. The presence of ceria is likely to contribute to the increase in fracture toughness. The sintered microstructure showed in Fig. 8 reveals dark and light regions corresponding to the mullite and zirconia grains, respectively. The presence of a small amount of residual porosity is also observed in a sintered microstructure. The fracture toughness is likely to be further enhanced as a result of the finer grain size in the mullite and ceria-stabilized zirconia resulting from sintering at the lower temperature of 1500°C. Metallographic analysis is planned in the future to quantify the grain size of the
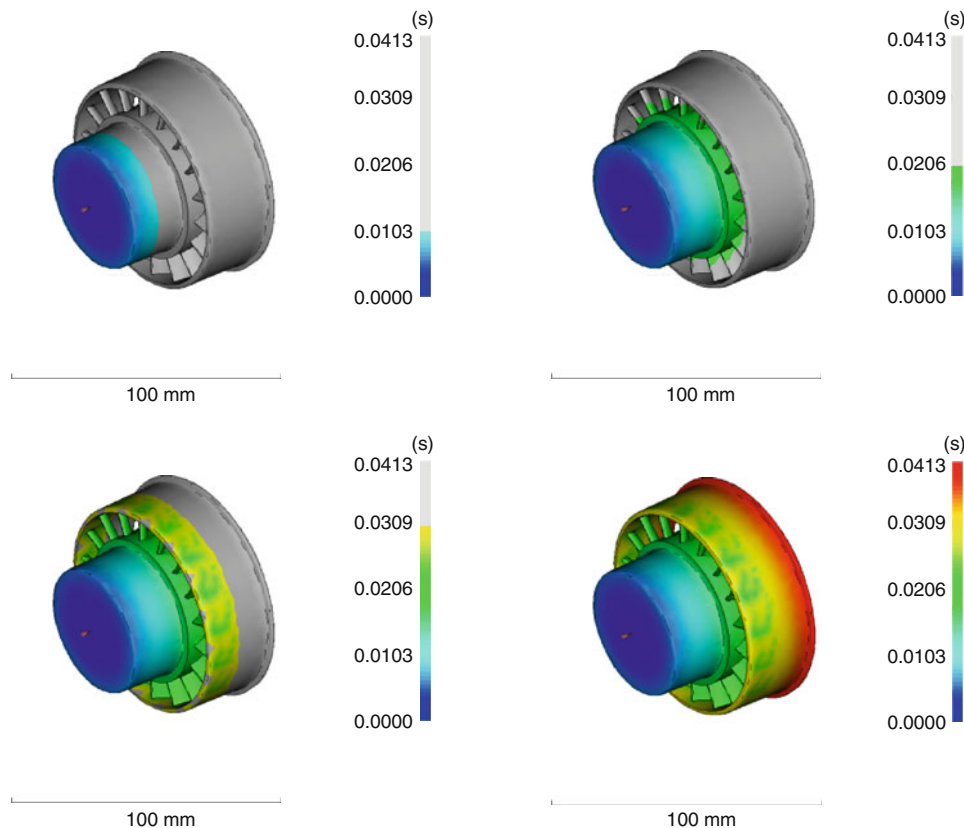

Fig. 9. Progressive mold filling of zirconia-toughened mullite feedstock for a miniature turbine stator geometry.

mullite and ceria-stabilized zirconia of the sintered samples.

Preliminary injection simulations were performed to investigate the feasibility of molding a stator component for a miniature turbine. Figure 9 shows the progressive filling of the selected geometry with the zirconia-toughened mullite feedstock. The Moldflow-recommended processing parameters were used for this initial study with a mold temperature of 23°C and a melt temperature of 150°C. With the specified stator geometry, molding was feasible over the entire melt and mold temperature range for the feedstock at fill times below 1.6 s. Although a feasible molding window exists, a preferred molding window was not found for any combination of injection time and melt and mold temperature. Injection pressure and cooling time were set automatically for the analysis, and so adjustment of these parameters will be needed in future studies to determine an optimum window for part quality. The information presented in Table III shows that mullite-zirconia composites are shaped either by tape casting, infiltration method, or uniaxial or isostatic pressing. Unlike PIM, these technologies do not have the capability of fabricating the complex-shaped parts required for high-performance applications. The present study confirms the potential ability of PIM to manufacture complex-shaped parts requiring enhanced properties.

CONCLUSIONS

Zirconia-toughened mullite components sintered to 97% density and 16.5% uniform shrinkage were successfully processed by PIM. The feedstock viscosity was less than 10^3 Pa s for the range of operating shear rates, indicating that the feedstock is suitable for injection molding. Furthermore, the successful molding of millimeter-scale features indicates that the feedstock is suitable for further investigations to fabricate geometrically complex components. Computer simulations on the mold-filling behavior using experimentally measured rheological and thermal characteristics of the feedstock also supported the potential for fabricating miniature turbine stators for UAVs. The feedstock property measurements were used to understand the mold-filling attributes of ceria-stabilized, zirconia-toughened mullite in the early stages of the design cycle and are reported in the literature for the first time to our knowledge. The fracture toughness (K_c) of the sintered zirconia-toughened mullite specimens (4.3 ± 0.3 MPa m$^{1/2}$) fabricated by PIM in this study was higher than that previously reported in the literature on simple geometries fabricated by uniaxial or isostatic pressing. The combined enhancement in sintered attributes and shape complexity of PIM observed in the present study increases the number of potential applications for zirconia-toughened mullite composites such as in the case of miniature turbine stators for unmanned aviation vehicles.

REFERENCES

1. J. Lenz, R.K. Enneti, V.P. Onbattuvelli, K.H. Kate, R. Martin, and S. Atre, *JOM* 388–392 (2012).
2. R. Kamo and W. Bryzik, SAE Paper 790645, 1979.
3. R.R. Sekar, R. Kamo, and J.C. Wood, SAE Paper 840834, 1984.
4. V.P. Onbattuvelli, R.K. Enneti, S.J. Park, and S.V. Atre, *Int. J. Refract. Met. Hard Mater.* 36, 77 (2013).
5. K.H. Kate, V.P. Onbattuvelli, R.K. Enneti, S.W. Lee, S.J. Park, and S.V. Atre, *JOM* 64, 1048 (2012).
6. V.P. Onbattuvelli, S. Vallury, T. McCabe, S.J. Park, and S.V. Atre, *Powder Inj. Mould. Int.* 4, 64 (2010).
7. K.H. Kate, R.K. Enneti, V.P. Onbattuvelli, and S.V. Atre, *Ceram. Int.* 38, 6495 (2013).
8. V.P. Onbattuvelli, R.K. Enneti, and S.V. Atre, *Ceram. Int.* 38, 6495 (2012).
9. R.K. Enneti, S.J. Park, A. Schenck, R.M. German, P. Thomas, B. Levenfeld, A. Várez, I.O. Palagi de Souza, J.P. de Souza, A.M. Fuentefria, V.P. Onbattuvelli, and S.V. Atre, *Int. J. Powder Metall.* 48, 23 (2012).
10. R.M. German, *Int. J. Powder Metall.* 36, 31 (2000).
11. G. Aggarwal, S.J. Park, and I. Smid, *Int. J. Refract. Met. Hard Mater.* 24, 253 (2006).
12. D.F. Heaney, *Handbook of Metal Injection Molding* (Cambridge: Woodhead Publishing Limited, 2012).
13. B.A. Bender and M.J. Pan, Mechanical Properties and Performance of Engineering Ceramics and Composites IV—33rd. *International Conference on Advanced Ceramics and Composites*, vol. 30, 2010, pp. 167–75.
14. K. Okada, N. Otsuka, R.J. Brook, and A.J. Moulson, *J. Am. Ceram. Soc.* 72, 2369 (1989).
15. M. Imose, A. Ohta, Y. Takano, M. Yoshinaka, K. Hirota, and O. Yamaguchi, *J. Am. Ceram. Soc.* 1050 (1998).
16. M.J. Vick, A. Heyes, and K. Pullen, *J. Eng. Gas Turbines Power* 132, 092301 (2010).
19. L. Kowalski and J. Duszczyk, *J. Mater. Sci.* 18, 1417 (1999).
20. C. Nylund and K. Meinander, *Heat Mass Transfer* 41, 428 (2005).
21. J. Shah and R.E. Nunn, *Powder Metall. Int.* 19, 38 (1987).
22. L. Liu, N.H. Loh, B.Y. Tay, S.B. Tor, Y. Murakoshi, and R. Maeda, *Mater. Charact.* 54, 230 (2005).
17. V.P. Onbattuvelli, (Ph.D Dissertation, Oregon State University, 2010).
18. L. Kowalski, J. Duszczyk, and L. Katgerman, *J. Mater. Sci.* 34, 1 (1999).
23. S.Laddha, (Ph.D Dissertation, Oregon State University, 2008).
24. L.B. Garrido, E.F. Aglietti, L. Martorello, M.A. Camerucci, and A.L. Cavalieri, *Mater. Sci. Eng. A* 419, 290 (2006).
25. J.S. Moya and M.I. Osendi, *J. Mater. Sci.* 19, 2909 (1984).
26. F. Sahnoune, N. Saheb, and P. Goeuriot, *Adv. Mater. Res.* 160–162, 1772 (2010).
27. J. Shyu and Y. Chen, *J. Mater. Res.* 10, 63 (1995).
28. S. Maitra, R. Chatterjee, S. Das, and A. Rahaman, *J Aust. Ceram. Soc.* 42, 71 (2006).
29. M.K. Haldar, T.K. Pal, and G. Banerjee, *Ceram. Int.* 28, 311 (2002).
30. J. Moran, T. Kelly, S. McKenna Lawlor, and J.A. Slevin, *Key Eng. Mater.* 32, 57 (1991).
31. S. Bodhak, S. Bose, and A. Bandyopadhyay, *J. Am. Ceram. Soc.* 94, 32 (2011).
32. D.M. Bigg and R.G. Barry, *Proceedings of the 1998 56th Annual Technical Conference*, vol. 1, 1998, pp. 997–1000.